Research Article | Vol. 25, No. 8 | 17 Apr 2017 | OPTICS EXPRESS A361

Optics EXPRESS

From toes to top-of-atmosphere: Fowler's Sneaker Depth index of water clarity for the Chesapeake Bay

BENJAMIN CROOKE,[1,2] LACHLAN I. W. MCKINNA,[1,3,*] AND IVONA CETINIĆ[1,4]

[1]*NASA Goddard Space Flight Center, Code 616, Greenbelt, MD 20771, USA*
[2]*Sandy Spring Friends School, Sandy Spring, MD, 20860, USA*
[3]*Science Applications International Corporation, McLean, VA 22102, USA*
[4]*GESTAR/Universities Space Research Association, Columbia, MD 21046, USA*
**lachlan.i.mckinna@nasa.gov*

Abstract: Fowler's Sneaker Depth (FSD), analogous to the well known Secchi disk depth (Z_{sd}), is a visually discerned citizen scientist metric used to assess water clarity in the Patuxent River estuary. In this study, a simple remote sensing algorithm was developed to derive FSD from space-borne spectroradiometric imagery. An empirical model was formed that estimates FSD from red-end remote sensing reflectances at 645 nm, $R_{rs}(645)$. The model is based on a hyperbolic function relating water clarity to $R_{rs}(645)$ that was established using radiative transfer modeling and fine tuned using in-water FSD measurements and coincident $R_{rs}(645)$ data observed by NASA's Moderate Resolution Imaging Spectroradiometer aboard the Aqua spacecraft (MODISA). The resultant FSD algorithm was applied to Landsat-8 Operational Land Imager data to derive a short time-series for the Patuxent River estuary from January 2015 to June 2016. Satellite-derived FSD had an inverse, statistically significant relationship ($p<0.005$) with total suspended sediment concentration (TSS). Further, a distinct negative relationship between FSD and chlorophyll concentration was discerned during periods of high biomass (> 4 μg L^{-1}). The complex nature of water quality in the mid-to-upper Chesapeake Bay was captured using a MODISA-based FSD time series (2002-2016). This study demonstrates how a citizen scientist-conceived observation can be coupled with remote sensing. With further refinement and validation, the FSD may be a useful tool for delivering scientifically relevant results and for informing and engaging local stakeholders and policy makers.

OCIS codes: (010.4450) Oceanic optics; (280.4991) Passive remote sensing; (010.5620) Radiative transfer.

References and links

1. M. Doron, M. Babin, O. Hembise, A. Mangin, and P. Garnesson, "Ocean transparency from space: validation of algorithms estimating Secchi depth using MERIS, MODIS and SeaWiFS data," Remote Sens. Environ. **115**(12), 2986–3001 (2011).
2. J. F. Knight and M. L. Voth, "Application of MODIS imagery for intra-annual water clarity assessment of Minnesota lakes," Remote Sens. **4**(12), 2181–2198 (2012).
3. Z. Lee, S. Shang, C. Hu, K. Du, A. Weidemann, W. Hou, J. Lin, and G. Lin, "Secchi disk depth: a new theory and mechanistic model for underwater visibility," Remote Sens. Environ. **169**, 139–149 (2015).
4. S. Weeks, P. Werdell, B. Schaffelke, M. Canto, Z. Lee, J. Wilding, and G. Feldman, "Satellite-derived photic depth on the Great Barrier Reef: spatio-temporal patterns of water clarity," Remote Sens. **4**(12), 3781–3795 (2012).
5. M. R. Wernand, H. J. van der Woerd, and W. W. C. Gieskes, "Trends in ocean colour and chlorophyll concentration from 1889 to 2000, worldwide," PLoS One **8**(6), e63766 (2013).
6. M. Haklay, "Citizen science and volunteered geographic information: overview and typology of participation," in *Crowdsourcing Geographic Knowledge: Volunteered Geographic Information (VGI) in Theory and Practice*, D. Sui, S. Elwood, and M. Goodchild, eds. (Springer Netherlands, 2013), pp. 105–122.
7. M. Thiel, M. Penna-Díaz, G. Luna-Jorquera, S. Salas, J. Sellanes, and W. Stotz, "Citizen scientists and marine research: volunteer participants, their contributions, and projection for the future," in *Oceanography and Marine Biology*, R. N. Hughes, D. J. Hughes, and I. P. Smith, eds. (Taylor and Francis, 2014), pp. 257–314.
8. J. L. Williams, S. J. Pierce, M. Fuentes, and M. Hamann, "Effectiveness of recreational divers for monitoring sea turtle populations," Endanger. Species Res. **26**(3), 209–219 (2015).

#283085 https://doi.org/10.1364/OE.25.00A361
Journal © 2017 Received 22 Dec 2016; revised 24 Feb 2017; accepted 6 Mar 2017; published 21 Mar 2017

Optics EXPRESS

9. N. J. Marshall, D. A. Kleine, and A. J. Dean, "CoralWatch: education, monitoring, and sustainability through citizen science," Front. Ecol. Environ **10**(6), 332–334 (2012).
10. S. P. Garaba, A. Friedrichs, D. Voß, and O. Zielinski, "Classifying natural waters with the Forel-Ule Colour index system: results, applications, correlations and crowdsourcing," Int. J. Environ. Res. Public Health **12**(12), 16096–16109 (2015).
11. J. A. Busch, I. Price, E. Jeansou, O. Zielinski, and H. J. van der Woerd, "Citizens and satellites: Assessment of phytoplankton dynamics in a NW Mediterranean aquaculture zone," Int. J. Appl. Earth. Obs. **47**, 40–49 (2016).
12. R. Horne, "Seeking sailors to help measure phytoplankton populations," Proc. Natl. Acad. Sci. U.S.A. **110**(18), 7107 (2013).
13. T. Leeuw, *Crowdsourcing water quality data using the iPhone camera*, MS Thesis (University of Maine, 2014).
14. W. Buytaert, Z. Zulkafli, S. Grainger, L. Acosta, T. C. Alemie, J. Bastiaensen, B. De Bièvre, J. Bhusal, J. Clark, A. Dewulf, M. Foggin, D. M. Hannah, C. Hergarten, A. Isaeva, T. Karpouzoglou, B. Pandeya, D. Paudel, K. Sharma, T. Steenhuis, S. Tilahun, G. Van Hecken, and M. Zhumanova, "Citizen science in hydrology and water resources: opportunities for knowledge generation, ecosystem service management, and sustainable development," Front. Earth Sci. **2**, 26 (2014).
15. W. M. Kemp, W. R. Boynton, J. E. Adolf, D. F. Boesch, W. C. Boicourt, G. Brush, J. C. Cornwell, T. R. Fisher, P. M. Glibert, J. D. Hagy, L. W. Harding, E. D. Houde, D. G. Kimmel, W. D. Miller, R. I. E. Newell, M. R. Roman, E. M. Smith, and J. C. Stevenson, "Eutrophication of Chesapeake Bay: historical trends and ecological interactions," Mar. Ecol. Prog. Ser. **303**, 1–29 (2005).
16. A. R. Zimmerman and E. A. Canuel, "A geochemical record of eutrophication and anoxia in Chesapeake Bay sediments: anthropogenic influence on organic matter composition," Mar. Chem. **69**(1-2), 117–137 (2000).
17. M. Langland and T. Cronin, *A summary report of sediment processes in Chesapeake Bay and watershed, USGS Water-Resources Investigations Report 03–4123*, (USGS, 2003).
18. W. R. Boynton, J. D. Hagy, J. C. Cornwell, W. M. Kemp, S. M. Greene, M. S. Owens, J. E. Baker, and R. K. Larsen, "Nutrient budgets and management actions in the Patuxent River estuary, Maryland," Estuaries Coasts **31**(4), 623–651 (2008).
19. C. F. D'Elia, W. R. Boynton, and J. G. Sanders, "A watershed perspective on nutrient enrichment, science, and policy in the Patuxent River, Maryland: 1960-2000," Estuaries **26**(2), 171–185 (2003).
20. D. R. Heinle, C. F. D'Elia, J. L. Taft, J. S. Wilson, M. Cole-Jones, A. B. Caplins, and L. E. Cronin, *Historical review of water quality and climatic data from Chesapeake Bay with emphasis on effects of enrichment, USEPA Chesapeake Bay Program Final report, No. 84*, (1980).
21. Maryland Department of Planning, *Patuxent River policy plan: a land management strategy*, (1984).
22. Maryland Department of Planing, retrieved 10 August, 2016, *http://planning.maryland.gov/OurWork/FowlerWadeIn.shtml*.
23. S. Gasteyer, C. B. Flora; Stephen Gasteyer, Cornelia Butler F, "Measuring ppm with tennis shoes: science and locally meaningful indicators of environmental quality," Soc. Nat. Resour. **13**(6), 589–597 (2000).
24. Marlyand Sea Grant, "An early Wade-In along Maryland's Patuxent River" (YouTube, 10 Feb 2017, 2015), retrieved *https://youtu.be/zfDIoKsvBiQ*.
25. Maryland Planning Department, "A conversation with Bernie Fowler on the occasion of the 25th annual Patuxent River Wade-in" (2012), retrieved 10 February 2017, *https://youtu.be/x_Zvu7zy2Pc*.
26. C. L. Gallegos, P. J. Werdell, and C. R. McClain, "Long-term changes in light scattering in Chesapeake Bay inferred from Secchi depth, light attenuation, and remote sensing measurements," J. Geophys. Res-Oceans **116**, 7160 (2011).
27. M. Wang, S. Son, and L. W. Harding, "Retrieval of diffuse attenuation coefficient in the Chesapeake Bay and turbid ocean regions for satellite ocean color applications," J. Geophys. Res-Oceans **114**, 1–15 (2009).
28. C. Le, C. Hu, J. Cannizzaro, and H. Duan, "Long-term distribution patterns of remotely sensed water quality parameters in Chesapeake Bay," Estuar. Coast. Shelf Sci. **128**, 93–103 (2013).
29. P. Wang, L. C. Linker, and R. A. Batiuk, "Monitored and modeled correlations of sediment and nutrients with Chesapeake Bay water clarity," J. Am. Water Resour. Assoc. **49**, 1103–1118 (2013).
30. Z. Chen, C. Hu, and F. Muller-Karger, "Monitoring turbidity in Tampa Bay using MODIS/Aqua 250-m imagery," Remote Sens. Environ. **109**(2), 207–220 (2007).
31. R. L. Miller and B. A. McKee, "Using MODIS Terra 250 m imagery to map concentrations of total suspended matter in coastal waters," Remote Sens. Environ. **93**(1-2), 259–266 (2004).
32. C. D. Mobley and L. K. Sundman, *Hydrolight 5 Ecolight 5 users' guide* (Sequoia Scientific 2008).
33. IOCCG, *Remote sensing of inherent optical properties: fundamentals, tests of algorithms, and applications*, (IOCCG, 2006).
34. B. A. Franz, S. W. Bailey, N. Kuring, and P. J. Werdell, "Ocean color measurements with the Operational Land Imager on Landsat-8: implementation and evaluation in SeaDAS," J. Appl. Remote Sens. **9**(1), 096070 (2015).
35. J. E. O'Reilly, S. Maritorena, B. G. Mitchell, D. A. Siegel, K. L. Carder, S. A. Garver, M. Kahru, and C. McClain, "Ocean color chlorophyll algorithms for SeaWiFS," J. Geophys. Res-Oceans **103**(C11), 24937–24953 (1998).
36. P. J. Werdell, B. A. Franz, S. W. Bailey, G. C. Feldman, E. Boss, V. E. Brando, M. Dowell, T. Hirata, S. J. Lavender, Z. Lee, H. Loisel, S. Maritorena, F. Mélin, T. S. Moore, T. J. Smyth, D. Antoine, E. Devred, O. H. d'Andon, and A. Mangin, "Generalized ocean color inversion model for retrieving marine inherent optical properties," Appl. Opt. **52**(10), 2019–2037 (2013).

Optics EXPRESS

37. G. Neukermans, H. Loisel, X. Mériaux, R. Astoreca, and D. McKee, "In situ variability of mass-specific beam attenuation and backscattering of marine particles with respect to particle size, density, and composition," Limnol. Oceanogr. **57**(1), 124–144 (2012).
38. USGS, "USGS current conditions for the nation ", retrieved 20 August, 2016, *http://waterdata.usgs.gov/usa/nwis/uv?01594440*.
39. Chesapeake Biological Laboratory Pier Monitoring Program, retrieved 20 August, 2016, *http://www.umces.edu/cbl/water-quality-data*.
40. Maryland Department of Natural Resources, "Eyes on the Bay", retrieved 10 August, 2016, *http://www.eyesonthebay.net*.
41. R. W. Preisendorfer, "Secchi disk science: visual optics of natural waters," Limnol. Oceanogr. **31**(5), 909–926 (1986).
42. C. D. Mobley, *Hydrolight Technical Note: How Secchi Depth is Computed* (Sequoia Scientific, 2004).
43. L. Alomassor, K. O'Donnell, and A. Carisio, *NOAA water level and meteorological data report: January 2016 Nor'easter*, (NOAA, 2016).
44. J. M. Testa, W. M. Kemp, W. R. Boynton, and J. D. Hagy III, "Long-term changes in water quality and productivity in the Patuxent River Estuary: 1985 to 2003," Estuaries Coasts **31**(6), 1021–1037 (2008).
45. T. R. Fisher, J. I. D. Hagy, W. R. Boynton, and M. R. Williams, "Cultural eutrophication in the Choptank and Patuxent estuaries of Chesapeake Bay," Limnol. Oceanogr. **51**(1part2), 435–447 (2006).
46. G. Zheng, P. M. DiGiacomo, S. S. Kaushal, M. A. Yuen-Murphy, and S. Duan, "Evolution of sediment plumes in the Chesapeake Bay and implications of climate variability," Environ. Sci. Technol. **49**(11), 6494–6503 (2015).
47. S. S. Kaushal, P. M. Mayer, P. G. Vidon, R. M. Smith, M. J. Pennino, T. A. Newcomer, S. Duan, C. Welty, and K. T. Belt, "Land use and climate variability amplify carbon, nutrient, and contaminant pulses: a review with management implications," J. Am. Water Resour. Assoc. **50**(3), 585–614 (2014).

1. Introduction

Historically, the aquatic remote-sensing community has focused on developing algorithms that can quantify in-water optical parameters with the best-possible precision and accuracy. Whilst these may be fit for the purpose of scientific research or environmental management, many satellite-derived parameters are conceptually abstract and not easily interpretable by the general public. This is due, in part, to the anticipated audience/data users who are often focused on complex scientific problems, and less so on general public interest or actual societal needs. Nonetheless, remote-sensing data can complement more rudimentary *in situ* observations, such as the Secchi disk depth (Z_{sd}) [1–4] and the Forel-Ule Color Index [5], to help study long-term spatiotemporal variability in marine optical conditions.

Members of the general public who volunteer to participate in scientific research are known as "citizen scientists" [6, 7]. In marine science, citizen scientists have been key to a number of studies on topics such as marine litter, seabirds, marine mammals, and coastal habitat condition [7]. Increasingly, academic researchers are collecting large amounts of scientific observations, or "crowdsourcing" data, by actively working with citizen scientists at geographical scales spanning from the local (e.g. SCUBA surveys of sea turtles [8]) to the global (e.g. CoralWatch [9]). It is important to note that citizen scientist activities can extend well beyond crowdsourcing to the interpretation and analysis of data, and even the defining of research questions and the collaborative design of scientific studies [6].

Optical observations of environmental conditions by citizen scientists are growing more useful for monitoring marine ecosystem health. To improve spatiotemporal observations of water clarity (turbidity), the broader community is increasingly being encouraged to take their own measurements based on user-friendly guidelines established by scientists [2, 10]. Indeed, a number of smart phone apps and websites have been established to encourage data crowdsourcing by the broader community (e.g. Citclops/EyeOnWater [11], Secchi Disk Project [12] and HydroColor [13]). Citizen scientist observations in environmental sciences are typically based on low cost, robust, straightforward and easily interpretable methods. Motivations for such observations are numerous, driven mostly by the need of immersion to the scientific process, sometimes resulting in participation in the decision making process from the "bottom-up" perspective [14].

The Chesapeake Bay, centered on 38.1°N 76.2°E, is a large estuary located in the mid-Atlantic region of the USA. It has a length of nearly 300 km and a surface area spanning

11,500 km^2 [15]. Sediment cores and direct observations have provided evidence that water quality in Chesapeake Bay has declined over the past 200 years as a direct consequence of watershed land use changes [15, 16]. Specifically, land clearing, agricultural practices, and urban development in the watershed have led to increased suspended sediment loads, excess nutrients (nitrogen and phosphorus), sewage, and other pollutants being transported into the Bay via rivers [15, 17]. This in turn has had a detrimental impact on ecosystem health leading to eutrophication, increased turbidity, decline in benthic vegetation, and deep-water hypoxia [15].

The Patuxent River is the sixth largest sub-estuary in the Chesapeake Bay, and discharges the seventh largest volume of freshwater [18]. It is located on the western side of the Bay and has a watershed spanning approximately 2,600 km^2, wholly situated within the state of Maryland. From the 1950s onwards, population growth in the watershed led to a marked decline in water quality [19]. This was particularly noticeable when reviewing historical Z_{sd} measurements collected in the lower Patuxent River [19, 20]. These data showed water clarity conditions in mesohaline waters during 1960/70's were markedly poorer than in the 1930s [20]. Throughout the 1970s community awareness about declining water quality and ecosystem health helped shape environmental policy. Indeed, in the 1980's statutory measures were enacted to improve water quality in the Patuxent River and comprehensive watershed management guidelines were established [19, 21].

Retired Maryland State Senator Bernie Fowler, a key figure associated with water quality improvement in the area, with the support of Tom Wisner, a local school teacher, conceived an engaging citizen scientist observation: the "Sneaker Index" [22, 23]. Akin to Z_{sd}, the Sneaker Index gives a visual appraisal of water column clarity by recording the depth at which the observer's white shoes are no longer visible [24, 25]. Figure 1 shows Senator Bernie Fowler (Ret.) and his white sneakers. Although distinctly similar to Z_{sd}, the Sneaker Index was conceived as a public awareness tool apparently with little consideration of the Secchi disk method [23]. Motivated by his concern for water clarity in the Patuxent River, and in hope to observe improved conditions after watershed improvement measures were set in place, every June since 1988 Senator Bernie Fowler (Ret.) holds annual Patuxent River 'wade-in' events [25]. Not only have the annual wade-ins provided a fun and engaging way to raise awareness of water quality changes to the general public, they have also resulted in a 28-year record of water clarity. However powerful due to their longevity, these observations are just a snapshot of the highly variable system, and as such susceptible to short-scale variability (e.g. windy day), and are unable to resolve intra- and inter-annual spatial variability.

The objective of this paper was to develop a simple method for observing the Sneaker Index, hereby referred to as "Fowler's Sneaker Depth" (FSD), from remotely sensed imagery. The FSD serves as a useful way to communicate aquatic remote sensing concepts with citizen scientists. In particular, as an already familiar concept, remotely sensed FSD could potentially be used to discuss spatial patterns of turbidity in the Patuxent River with the general public. We also examine the potential of satellite derived FSD for resolving intra- and inter-annual variability in regional water clarity. We acknowledge that a number of other studies have used remote sensing to observe trends in water quality parameters in the Chesapeake Bay [26–28], however, none of these have derived a citizen scientist water clarity metric specifically developed by community water quality advocates. The primary driver of water clarity (turbidity) in the Patuxent River estuary, as in many parts other parts of the Chesapeake Bay, is total suspended solids (TSS; both volatile and inorganic material [17, 29]). In coastal and inland waters, the magnitude of the light reflected from the water-column at red wavelengths (e.g. remote-sensing reflectance at 645 nm, $R_{rs}(645)$) is often proportional to TSS concentration [30, 31]. Based on these assertions, we expect FSD to be dependent upon TSS concentration, and in turn, we assume that it may be possible to predict FSD from sensor-observed $R_{rs}(645)$. In the end, a proof-of-concept FSD algorithm is presented and

variability of FSD is evaluated over finer temporal scales for the Patuxent River estuary and the mid-to-upper Chesapeake Bay region.

Fig. 1. Retired Maryland State Senator Bernie Fowler in 2012 holding the white sneakers he wears at annual Patuxent River wade-in events. Image credit: Maryland Department of Planning [22].

2. Data and modeling

2.1 Fowler's Sneaker Depth data

In-water FSD measurements were collected at annual 'wade-ins' that have occurred on the second Sunday in June, from 1988 onwards. Participants slowly wade into a section of the Patuxent River, located on the western side of the Chesapeake Bay as shown in Fig. 2, until their white sneakers are no longer visible. Once this occurs, a wooden meter stick is used to measure the water-column depth in inches. FSD data were sourced from the Maryland Department of Planning website [22]. We note that annual wade-ins have occurred at two separate locations: Broomes Island (BI) from 1988 – 2009, and Jefferson Paterson Park (JPP) and from 2010 – present, both locations are indicated in Fig. 2. For this study we converted the FSD from inches to meters, and considered only years that MODIS Aqua (MODISA) was in orbit (2003 – 2016). Full details are given in Table 1.

It is important to acknowledge that annual wade-ins are community events devised for the purpose of raising public awareness. Thus, FSD data were never intended for use in satellite algorithm development and may lack some scientific rigor. For example, each year many participants, often numbering several hundred [25], attend the wade-ins. Accordingly, it is possible that some fine sediments are resuspended by foot traffic thereby adding uncertainty to FSD observations. Although, in a recorded video of the 1990 wade-in [24] when water clarity was 0.4m [22], sediment stirring by Bernie Fowler's white sneakers appears minimal. Further, because the wade-ins occur on a fixed date (second Sunday in June), environmental conditions that can influence water clarity, such as tidal forcing, are unlikely to be same year-to-year. Nonetheless, for the purpose of developing a simple satellite algorithm, we believe the FSD data has been collected with sufficient consistency to be of useful quality.

Optics EXPRESS

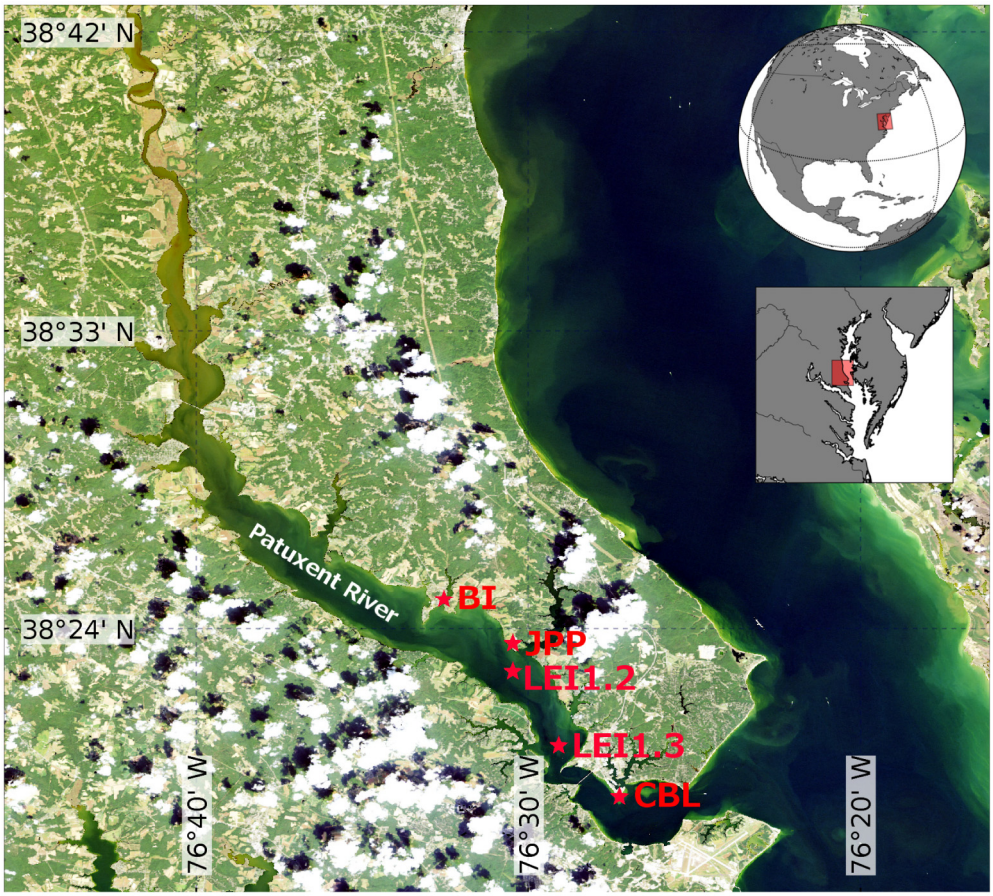

Fig. 2. Quasi-true color image of the Patuxent River estuary and adjacent Chesapeake Bay captured by Landsat-8 OLI on 18 September 2015. Waters near the river mouth appear greenish-yellow most likely due to an abundance of phytoplankton. Waters upstream from the river mouth are a distinct brown color, likely due to suspended mineral sediment. Annotated in red letters are the wade-in locations of Broomes Island (BI) and Jefferson Patterson Park (JPP), the monthly monitoring sites St Leonard (LEI.2) and Above Point Patience (LEI1.3), and the Chesapeake Bay Laboratory (CBL).

2.2 Radiative transfer modeling

To conceptualize how visually-discerned water clarity depth relates to $R_{rs}(645)$, a brief radiative transfer study was performed. Specifically, Hydrolight-Ecolight 5 (HE5) radiative transfer code [32] was used to theoretically calculate Z_{sd} and $R_{rs}(645)$ for a range of water-column optical conditions. Our underlying assumption was that that any relationship between Z_{sd} and $R_{rs}(645)$ would be similar to that of FSD and $R_{rs}(645)$. A set of 575 inherent optical properties (IOPs) were synthesized using the methodology of IOCCG [33]. These IOP combinations spanned a range of optical conditions from pure seawater – defined by an absence of chlorophyll (Chl) through to highly turbid conditions (100 µg Chl L^{-1}). For brevity, we will not detail how we parameterized HE5 radiative transfer software (i.e. atmospheric, surface, and the water-column conditions) as these details are described elsewhere [33].

Using the simulated HE5 data set, it was possible to develop a mathematical model to predict water clarity depth (i.e. Z_{sd}) as a function of $R_{rs}(645)$. To determine how well the mathematical model fit the data, appropriate metrics were used to compare modeled water

Optics EXPRESS

clarity depth (i.e Z_{sd} or FSD), $\hat{Z}$, with known (i.e. HE5-modeled or *in situ*) water clarity depth, *Z*. Specifically, we used the linear regression metrics of r-squared and regression slope to assess model fit. The median ratio (MR) was used to assess bias, where

$$MR = median\left[\hat{Z}_i / Z_i\right]. \quad (1)$$

2.3 Satellite imagery

2.3.1 Concurrent MODISA imagery

Level-1 MODISA data were downloaded from NASA Ocean Biology Distributed Active Archive Center's website (OB.DAAC: http://oceancolor.gsfc.nasa.gov/) and processed using NASA's L2GEN processing code that is distributed as part of the SeaDAS ocean-color display and analysis software suite (http://seadas.gsfc.nasa.gov/). Values of $R_{rs}(645)$ and Rayleigh-corrected radiances, $\rho_s(\lambda)$, were derived. We note that the 645 nm band of MODISA is the only visible band of the sensor with 250 m x 250 m resolution making it suitable for observing narrow sub-kilometer scale channels and estuaries of the Chesapeake Bay. For algorithm development, it is best practice to have satellite overpass dates coincident with *in situ* data collection dates. However, due to effects such as thick cloud cover, sunglint, and orbit gaps, MODISA data was not always available at the time of wade-ins. Accordingly, we used MODISA data ± 1 day on either side of wade-ins, when coincident images were unavailable, in order to maximize the number of data points (see Table 1). We note that the standard land masking procedure used in L2GEN obscured the Patuxent River estuary. Thus, for algorithm development purposes, the default land mask was switched off during L2GEN processing.

After L2GEN processing was complete, output level-2 files were visually inspected one-by-one using SeaDAS software. For each file, $R_{rs}(645)$ was displayed, and a custom coastline and landmask was generated using 150 m resolution NASA Shuttle Radar Topographic Mission Global Coverage (SRTM_GC) data. Next, quasi-true color images were generated using the $\rho_s(645)$, $\rho_s(555)$, and $\rho_s(469)$ (red, green, and blue) bands. By inspecting the land/coastline mask and quasi-true color imagery together it was possible to discern the Patuxent River and visually determine the quality of $R_{rs}(645)$ data. If the scene was clear and of good quality, the SeaDAS geometry tool was used to draw a 5 x 5 pixel box nearest to the wade-in sites. Care was taken to ensure the box did not contain land pixels. The SeaDAS statistics tool was then used to calculate the mean, median and standard deviation of the 5 x 5 boxed regions.

Environmental factors that affect turbidity, such as tide, may differ between the wade-in and the time of satellite overpass. Although the Patuxent River estuary experiences micro-tidal conditions, we still examined the difference in tide height between the time of wade-in (approximately 14:00) and satellite overpass. For this study, no direct record of tides was available for BI and JPP. Instead, we used NOAA tidal harmonics for nearby CBL (NOAA station 8577330) to calculate tide height relative to mean sea level (MSL). These data, shown in Table 2, indicate that for most years tidal situations were comparable with absolute differences usually less than 0.20 m. However, we note that in 2013 and 2016 the absolute difference in tide height was 0.28 m and 0.30 m, respectively.

2.3.2 High resolution Landsat-8 imagery

The Operational Land Imager (OLI) aboard the Landsat-8 satellite provides data with 30 m x 30 m pixel resolution. This spatial resolution of OLI makes it ideal for observing fine-scale narrow inlets and estuaries of the Chesapeake Bay that are poorly resolved by MODISA [34]. OLI also provided a high quality satellite data set independent of MODISA suitable for evaluating the FSD algorithm. All OLI level-1 files that contained the Patuxent River estuary region were downloaded from the US Geological Survey (USGS) EarthExplorer website

Optics EXPRESS

(http://earthexplorer.usgs.gov/). This resulted in a total of 15 clear scenes spanning January 2015 – July 2016. All level-1 data were processed using L2GEN with the output level-2 files containing $R_{rs}(\lambda)$ and $\rho_s(\lambda)$ data. As for MODISA, the standard landmask was turned off during data processing. Each individual OLI image was assessed visually as for MODISA imagery (see section 2.3.1), and data were extracted for a small 5 x 5 pixel box nearest to JPP site.

Table 1. Details of in-water FSD wade-ins and MODISA satellite overpass

Wade-in date (dd/mm/yyy)	Location	Fowler Sneaker Depth [m]	Median MODIS $R_{rs}(645)$ [sr^{-1}]	MODIS $R_{rs}(645)$ Coefficient of Variation	± days of satellite overpass
08/06/2003	BI	0.62	0.0072[a]	2.42E-3	+ 1
13/06/2004	BI	0.80	0.0116	1.70E-03	+ 1
12/06/2005	BI	0.69	-	-	0
11/06/2006	BI	0.69	-	-	–1
10/06/2007	BI	0.53	0.0157	1.00E-3	–1
08/06/2008	BI	0.66	0.0140	8.58E-4	–1
14/06/2009	BI	0.64	0.0127	1.80E-3	0
13/06/2010	JPP	0.87	0.0096	3.86E-4	0
12/06/2011	JPP	0.79	-	-	0
10/06/2012	JPP	0.88	0.0094	4.12E-4	0
09/06/2013	JPP	0.86	0.0076	2.02E-4	–1
08/06/2014	JPP	0.58	0.0069[a]	1.80E-3	–1
14/06/2015	JPP	1.13	0.0086	2.05-4	0
12/06/2016	JPP	0.78	-	-	–1

[a]Suspected outlier.

Table 2. Details of tide height on wade-in days and during MODISA satellite overpass

Wade-in date (dd/mm/yyy)	Location	± days of satellite overpass	Satellite data available Yes/No	Tide[a] height at 2pm on day of wade-in [m]	Tide[a] height at overpass time [m]	Absolute difference between tide [m]
08/06/2003	BI	+ 1	Yes	0.19	0.14	0.05
13/06/2004	BI	+ 1	Yes	0.10	0.15	0.05
12/06/2005	BI	0	No	0.04	–0.07	0.11
11/06/2006	BI	–1	No	–0.07	0.13	0.20
10/06/2007	BI	–1	Yes	0.19	0.07	0.12
08/06/2008	BI	–1	Yes	0.04	–0.02	0.06
14/06/2009	BI	0	Yes	0.07	–0.07	0.14
13/06/2010	JPP	0	Yes	–0.12	–0.06	0.06
12/06/2011	JPP	0	No	0.14	0.18	0.04
10/06/2012	JPP	0	Yes	0.11	–0.01	0.12
09/06/2013	JPP	–1	Yes	–0.12	0.16	0.28
08/06/2014	JPP	–1	Yes	0.17	0.11	0.06
14/06/2015	JPP	0	Yes	0.02	0.13	0.11
12/06/2016	JPP	–1	No	0.17	–0.15	0.32

[a]Tide calculated for CBL; datum is mean sea level (MSL).

2.3.3 MODISA time-series

To determine the capability of FSD for observing decadal variability, the entire MODISA archive (2002 – 2016) was processed for the Chesapeake Bay region. Daily level-2 swath resolution (unmapped) data were produced using L2GEN, then files containing valid data were spatially aggregated to an equal area grid representation with standard pixel resolution of 500 m. These data were then temporally aggregated to a monthly resolution (n = 168).

Optics EXPRESS

From this monthly time-series, a sub-region was extracted encompassing the mid-to-upper Chesapeake Bay (30.6 – 37.9°N, 75.6 – 76.9°W). The MODISA-derived parameters used were $R_{rs}(645)$, Chl, and the particulate backscattering coefficient at 443 nm, $b_{bp}(443)$. Chl values were derived using the standard NASA algorithm [35] and $b_{bp}(443)$ values were derived using default configuration of the Generalized Inherent Optical Properties framework algorithm (GIOP) [36]. We note the magnitude of $b_{bp}(443)$ is typically considered directly proportional to TSS [37].

2.4 Environmental observations

To contextualize satellite-derived values of FSD with estuarine processes, we sourced *in situ* data of various environmental conditions. Hourly rates of Patuxent River discharge, measured at USGS station 01594440 near Bowie, MD were obtained from the USGS website [38]. Measurements of Chl were collected in 15 minute intervals by a YSI EXO2 probe at the University of Maryland's Center for Environmental Studies - Chesapeake Biological Laboratory (CBL) pier, as part of CBL Pier Monitoring Program [39]. Discrete measurements of Chl and total suspended sediments (TSS) at two monitoring stations located near the FSD wade-in sites: St Leonard (LEI1.2) and Above Point Patience (LEI1.3) were obtained from the Maryland Department of Natural Resources [40]. Discrete data samples were analyzed following the EPA approved methods. Locations of monitoring sites are shown in Fig. 2.

3. Results and discussion

3.1 Relating water clarity depth to $R_{rs}(645)$

The scatter plots in Fig. 3 show how simulated Z_{sd} monotonically decreases with increasing $R_{rs}(645)$ with asymptotic behavior occurring at both axes. It was determined that this relationship could be well represented using a hyperbolic function of the form

$$Z_{SD} = \frac{c_0}{c_1 R_{rs}(645)}. \tag{2}$$

Using non-linear least squares regression, the coefficients c_0 and c_1 were found to have values of 0.252 m and 20.0 sr, respectively. The linear regression statistics for the hyperbolic model were an r-squared value of 0.95, regression slope of 0.91 and median ratio of 1.09. Collectively, these statistics indicated that the hyperbolic model explains the relationship between Z_{sd} and $R_{rs}(645)$ with good precision and low bias. We note that the asymptotic behavior of the hyperbolic function may be problematic, particularly where very low values of $R_{rs}(645)$ may lead to large water clarity depths. Indeed, water clarity depths exceeding several meters are unlikely in turbid waters of the Chesapeake Bay. Accordingly, water clarity depths exceeding 12 m, the point at which asymptotic y-axis behavior begins, should be interpreted with caution. We also note for FSD, water clarity depths deeper than a person is tall cannot be validated via the existing wade-in methodology.

Because FSD is analogous to Z_{sd}, we postulated that Eq. (2) should be applicable for relating FSD to $R_{rs}(645)$. Using non-linear least squares regression we fitted the hyperbolic curve through the ten FSD data points that had coincident MODISA-observed $R_{rs}(645)$ data (see Table 1). Initial results revealed that the model performed poorly with an r-squared value of 0.04, a regression slope of 0.26, and a median ratio of 0.93. On closer inspection, two data points were deemed out-of-family; one of them having coefficient of variation greater than 20% (Table 1). These two data points (see red circle in Fig. 3) were excluded from further analysis. The curve was refit, and the linear regression statistics were much improved as evidenced by an r-squared of 0.68, a regression slope of 0.89, and a median ratio of 1.01. The corresponding hyperbolic fit coefficients c_0 and c_1 were 0.058 m and 6.83 sr respectively.

We wish to note that it is not surprising that the hyperbolic fit coefficients would differ between Z_{sd} and FSD. Particularly as observed FSD values are slightly smaller than modeled

Optics EXPRESS

Z_{sd} values. Whilst the two measurements are similar, the sampling protocols for Z_{sd} and FSD differ greatly which may, in part, explain differences between the two water clarity metrics. In particular, FSD is more intrusive than Z_{sd} as the observer has to physically enter the water to make a measurement. This presence of the observer's body in the water could potentially stir up sediments and, depending sun position, cause self-shading of the white sneakers. In addition, the way HE5 calculates Z_{sd} using the model of Preisendorfer [41] has its own underlying assumptions related, in part, to the photopic reflectance property of a white Secchi disk with a surface area of approximately 0.3 m^2 [42]. We concede that these assumptions may not hold for a pair of white sneakers with a surface of area of approximately 0.02 m^2.

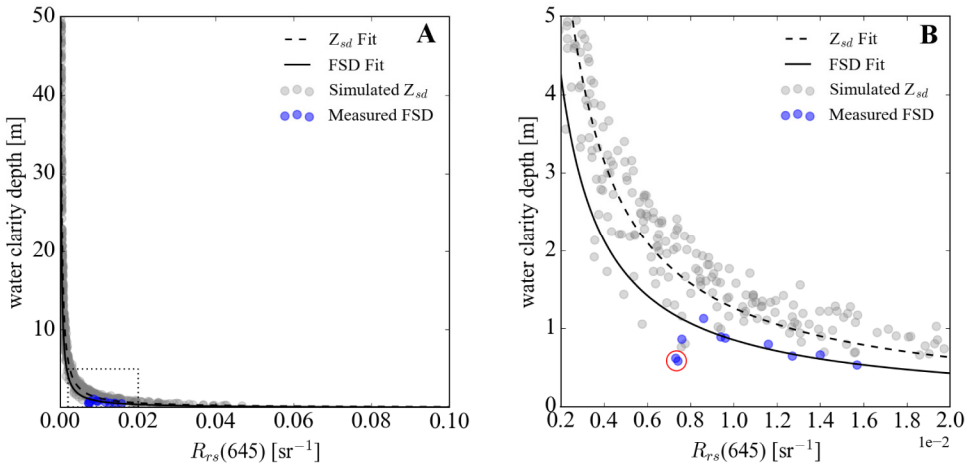

Fig. 3. Panel A shows simulated Z_{sd} (grey data points) varying with $R_{rs}(645)$. A region-of-interest box, defined by dotted line, surrounds in-water FSD data (blue data points) plotted against coincident MODISA-observed $R_{rs}(645)$. Panel B zooms in on the region-of-interest box showing the in-water FSD data points more clearly. A red line encircles two suspected outliers. In both panels, two best fit lines are displayed: a dashed line for Z_{sd} depth vs. $R_{rs}(645)$ and a solid line for FSD vs. $R_{rs}(645)$.

3.2 Sample FSD image

To demonstrate the utility of FSD for visualizing spatial patterns in water clarity, we processed a sample Landsat-8 OLI image of the Patuxent River estuary and part of the adjacent Chesapeake Bay. We selected an image captured on 24 January 2016 after an intense blizzard, dubbed "Winter Storm Jonas", had passed over the region [43]. During the storm, the Chesapeake Bay region was significantly impacted by heavy snowfall, strong winds, and a storm surge. From the derived FSD image, shown in Fig. 4(b), we can visualize the acute impact the storm had on water clarity, particularly at a time (mid-winter) when conditions are often considered to be clearest.

Figure 4(a) shows a quasi-true color image with land appearing white, due to aggregated snow. The waters of the upper Patuxent River estuary and the adjacent Chesapeake Bay are brown colored and highly turbid, presumably due to physical forcing (wind and storm surge action [43]) causing localized erosion and/or resuspension of sediments. Areas of the mid-to-lower Patuxent River Estuary appear dark colored suggesting the waters there are highly absorbing and/or lacking highly scattering particulate matter. The derived FSD image is shown in Fig. 4(b). FSD can be interpreted using a color scheme where warm colors correspond to turbid water and cool colors correspond to clearer water. Unsurprisingly the spatial patterns of FSD shown in Fig. 4(b) match well with brown colored water depicted Fig. 4(a).

The median FSD observed for the adjacent Chesapeake Bay was 0.62 m while for the upper Patuxent River estuary the median FSD was 0.70m. For the dark colored waters of the

Optics EXPRESS

mid-to-lower Patuxent River estuary (near BI and JPP), FSD had a median value of 2.0 m. We note that no coincident *in situ* water clarity observations were collected for direct comparison with satellite-derived values. However, five days later on 29 January 2016 routine water quality monitoring measured *in situ* Z_{sd} values at LEI1.2 and LEI1.3 of 2.1 m and 2.2 m, respectively. We note that OLI-derived FSD values for LE1.2 and LEI1.3 stations on 24 January were 2.4 m and 2.7 m, respectively. Although encouraging, this cursory comparison is not conclusive as FSD and Z_{sd} are not directly comparable and there were five days separating the satellite and *in situ* observations. Nonetheless, this example can be used effectively to communicate the concept of spatial heterogeneity in water clarity and also demonstrate how severe weather can impact water quality in the region.

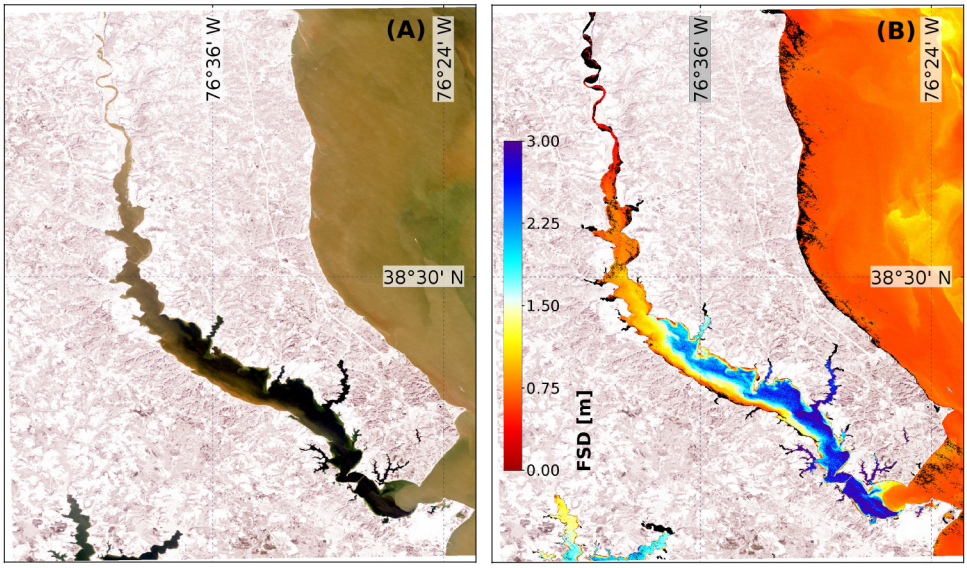

Fig. 4. Landsat-8 OLI imagery of the Patuxent River and adjacent Chesapeake Bay captured on 24 January 2016 following a severe winter storm. Panel A shows a quasi-true color image of the region. Highly turbid waters appear brown whilst clearer, less scattering waters are dark colored. Panel B shows FSD, the depth at which you can no longer see a pair of white sneakers, derived using Eq. (2). Black pixels in panel B correspond to invalid (bad data) pixels where atmospheric correction failure occurred.

3.3 Patuxent River time-series

A short FSD time-series (January 2015 – July 2016) was calculated from OLI $R_{rs}(655)$ data observed immediately adjacent to the JPP site. The time-series, shown in Fig. 5, demonstrates large intra- and inter-annual variability in water clarity. Direct measurements of FSD fit nicely in the OLI derived FSD time series. During winter months, FSD was deepest with a maxima of 11.82 m reached in December of 2015 coinciding with low TSS and Chl values as measured by the nearby LE1.2 and LE1.3 monitoring stations. We note, however, this deep FSD value cannot be directly validated. The shallowest FSD values were observed during late spring/early summer, timed near the annual wade-in, when highest TSS and Chl concentrations were measured at LE1.2 and LE1.3.

No correlation between the Patuxent River discharge rate and FSD was found. A statistically significant negative relationship was found between FSD and LEI1.2 TSS ($p<0.005$, r-squared = 0.85, n = 5, only the samples collected on the same day were used here), supporting the concept of FSD dependence on particle loads. The relationship between FSD and Chl seems to be a complex one; the discrete Chl samples collected at monitoring sites do not display a significant correlation with FSD. However, for the data set collected at

CBL pier, we found a statistically significant negative trend between FSD and Chl concentrations for the periods in which Chl concentrations exceeded 4 µg L^{-1} ($p = 0.054$, $r^2 = 0.72$).

Our results suggest that water clarity in the vicinity of JPP (mid-estuary), for most of the OLI-observed period, is driven by particulate matter of local origin probably eroded and/or resuspended sediment and detrital particles. During periods of increased Chl concentration (> 4 µg L^{-1}), control of water clarity seems to be driven by phytoplankton biomass, originating from the more saline (lower) part of the Patuxent River estuary. Indeed, despite a reduction in point source nutrient inputs in the Patuxent River watershed, summer phytoplankton blooms in the lower Patuxent River estuary have persisted [44]. Recent studies suggest that the dominant nutrient source driving this observed productivity has shifted from watershed-based to Chesapeake Bay-oriented [44, 45]. Our data do not have the temporal resolution needed to tease out the potential influence of tides on the observed trends. Cumulatively, our results complement contemporary understanding that water clarity seasonal reduction in the lower Patuxent River estuary is driven by an increase in phytoplankton biomass due to excess nutrient input and to the lesser extent by incoming inorganic sediment load.

Collectively the results suggest that the FSD algorithm is applicable to turbid waters that exhibit high optical scattering due to suspended particles or high phytoplankton biomass (> 4 µg L^{-1}). However, we concede that for low scattering (low turbidity) waters, the current FSD algorithm is likely to underperform. Under such circumstances, the signal at $R_{rs}(655)$ will be small and inputting such values into the hyperbolic model (Eq. (2)) may lead to unrealistically large FSD retrievals. This identifies an aspect for further algorithm improvement.

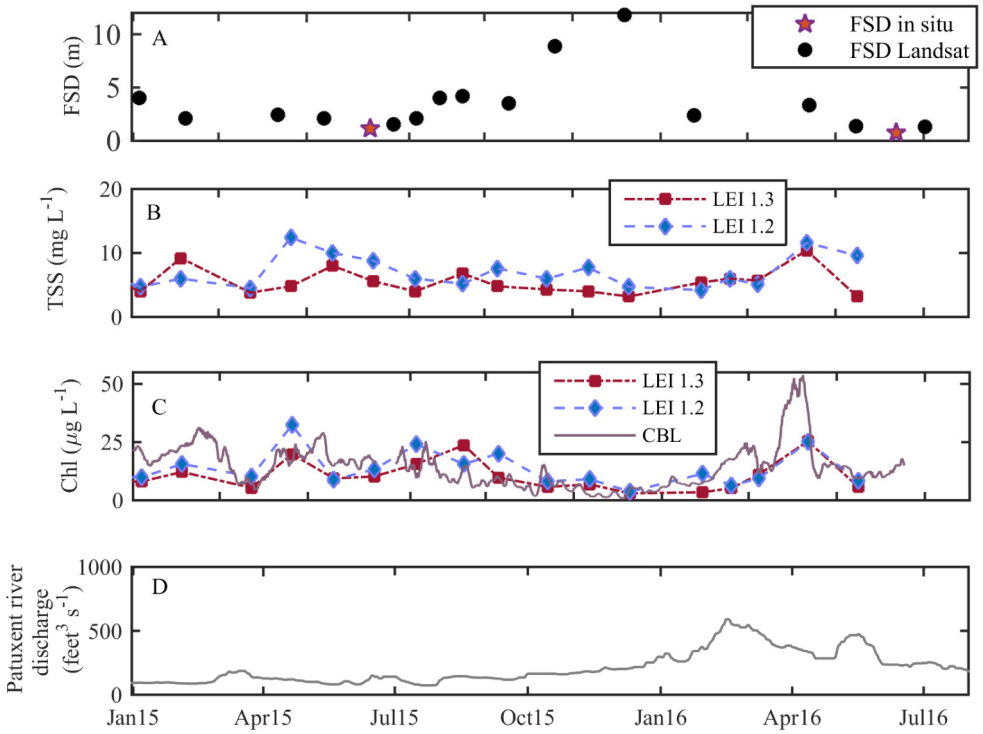

Fig. 5. Patuxent river time-series, panel A depicts FSD variability over the period of year and a half, for the sampling site (panel A), followed by the monthly variability of total suspended sediments on two monitoring stations in proximity of sampling site (panel B). Panel C is showing the chlorophyll variability on same monitoring stations (red and blue), and chlorophyll variability measured by the probe on CBL pier. Variability of the Patuxent River discharge is depicted on panel D.

Optics EXPRESS

3.4 Chesapeake Bay time-series

MODISA-derived FSD in Chesapeake Bay displays no significant long-term trends during the fourteen-year period of the MODISA mission. Median FSD for 2002-2016 period was 3.7 m, while the range was 1.7–7.2 m, with maximum and minimum FSDs encountered during 2015 and 2016. These extreme FSDs were encountered during the periods of lowest and highest particle loads, as respectively indicated by $b_{bp}(443)$ values; see Figs. 6(a) and 6(b). The presence of phytoplankton doesn't seem to co-vary with FSD, although decreases in the FSD are visible during the periods of high Chl concentrations (e.g., spring blooms of 2013, 2014; Figs. 6(a) and 6(b)). Comparison of in-water FSD collected in the Patuxent River estuary (purple stars, Fig. 6(a)) with MODISA derived monthly FSD demonstrate no correlation between these two systems, and FSD is significantly smaller in Patuxent River system (two-tailed t-test, $p<0.001$).

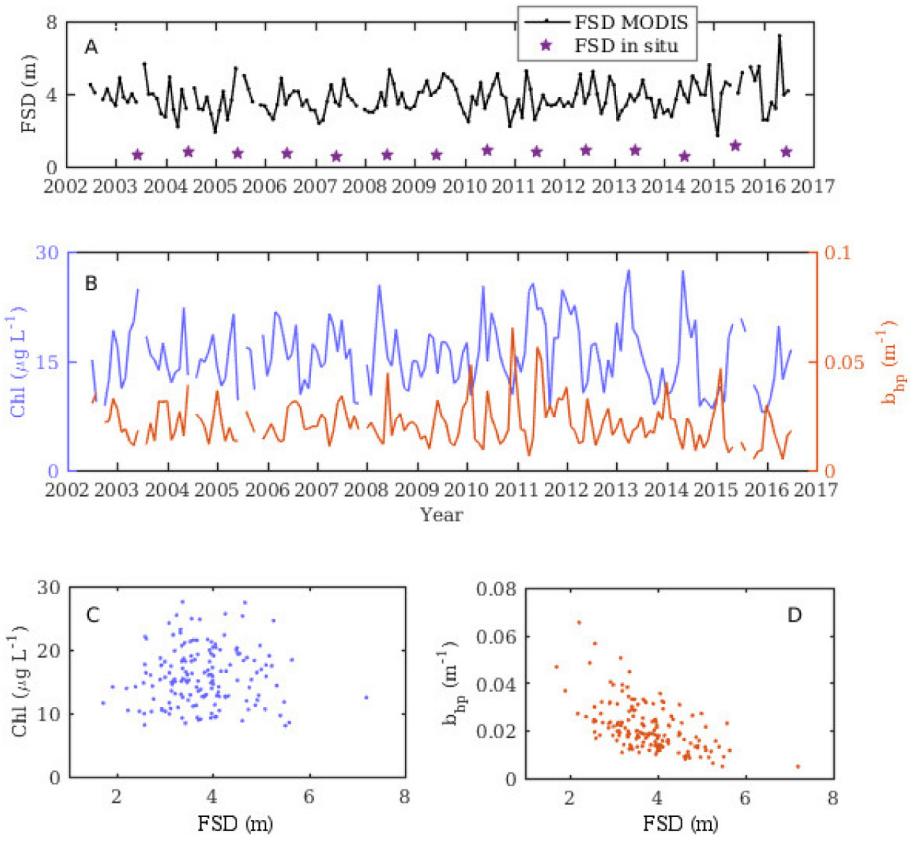

Fig. 6. Chesapeake Bay time-series, panel A depicts FSD variability over the MODISA mission, followed by the monthly variability of Chlorophyll a (blue) and backscattering (red) (panel B). FSD seems to co-vary with backscattering in the bay (Panel D), indicating that is more susceptible to the changes in sediment load than the chlorophyll concentration (Panel C).

Due to the nature of the algorithm, a strong correlation was expected between $b_{bp}(443)$ and FSD, however, our results yielded an r-squared value of 0.3 for the type II linear relationship, pointing to other sources controlling the water clarity of the upper-to-mid Chesapeake Bay. The Chesapeake Bay is a complex estuary and visibility in its upper part, due to the influence of the Susquehanna River sediment loading, acts in the similar way to Patuxent River [46]. However, in parts of the mid-to-upper Bay phytoplankton is controlling

Optics EXPRESS

water clarity. This may be reason that FSD is not performing well as a Bay-integrated metric for water clarity.

Interestingly, the MODISA time-series points to an increase in FSD amplitude during the last two years (2014-2016). Indeed, analysis revealed that the average FSD and its standard deviation has significantly increased for the 2014-2016 period, when compared to the rest of the mission (two tailed t-test, $p = 0.0095$). Similarly, increases in the magnitude of stream-flow variability (which is directly related to the sediment load) have also been noted in this area [47] and are attributed to changes in regional climate variability.

4. Conclusion

The Fowler Sneaker Depth is a citizen scientist metric of water clarity for the Patuxent River estuary. The FSD is conceptually easy to understand, and useful for communicating long-term trends in water clarity to the general public. However, because the citizen scientist-observed FSD is a discrete observation measured at one location once a year, intra- and inter-annual variability cannot be resolved. To address this concern, we developed a simple remote-sensing algorithm for deriving FSD with MODISA and/or Landsat-8 OLI imagery that was capable of resolving FSD variability at finer temporal scales. Our results presented here demonstrate how a community-based optical observation can be scaled-up to remote sensing. However, in this study we have assumed that highly scattering suspended particulate matter is the dominant driver of water clarity in the Patuxent River estuary. We acknowledge that this may lead to anomalously large FSD values under low scattering conditions. Accordingly, future algorithm refinement should consider strongly absorbing matter (i.e. CDOM and phytoplankton). Additionally, the FSD algorithm could be improved with the collection of more *in situ* FSD data, perhaps via a new citizen scientist crowdsourcing project. We expect that with further refinement and validation, the FSD algorithm could be used for (i) delivering scientifically-relevant results, (ii) engaging and educating local stakeholders, and (iii) informing policy makers.

Acknowledgments

The authors would like to thank the Chesapeake Biological Laboratory Pier Monitoring Program and Carlos Lozano for sharing their data with us. We are thankful to the Maryland Department of Planning for sharing freely the Sneaker Depth data set, USGS for freely sharing their Patuxent River discharge data, and the Maryland Department of Natural Resource for freely sharing their monitoring data. We wish to thank Dr Carlos del Castillo, the NASA Ocean Ecology Lab Chief, for providing the resources necessary for this work. We also wish to thank Tommy Owens for providing MODIS data processing support and Kitty Sanchez for administrative support relating to this project. The anonymous reviewer is also acknowledged for their highly useful comments. Finally, we wish to recognize the decades-long efforts of Senator Bernie Fowler (Ret.) as a staunch advocate for improving water quality and ecosystem health of the Chesapeake Bay.